Axial electric wake field inside the induction gap exited by the intense electron beam*

ZHANG Kai-Zhi(张开志)[1)] ZHANG Huang(张篁) LONG Ji-Dong(龙继东)
YANG Guo-Jun(杨国君) HE Xiao-Zhong(何小中) WANG Hua-Cen(王华岑)

(Institute of Fluid Physics, CAEP, Mianyang 621900, China)

Abstract While an intense electron beam passes through the accelerating gaps of a linear induction accelerator, a strong wake field will be excited. In this paper a relatively simple model is established based on the interaction between the transverse magnetic wake field and the electron beam, and the numerical calculation in succession generates a magnetic wake field distribution along the accelerator and along the beam pulse as well. The axial electric wake field is derived based on the relation between field components of a resonant mode. According to some principles in existence, the influence of this field on the high voltage properties of the induction gap is analyzed. The Dragon-I accelerator is taken as an example, and its maximum electric wake field is about 17 kV/cm, which means the effect of the wake field is noticeable.

Key words linear induction accelerator, induction gap, wake field, high voltage breakdown property

PACS 52.59Mv, 29.17.+w, 29.25.Bx

1 Introduction

Electrical breakdown property is one of the main considerations in the design of an induction accelerating cell[1]. Traditionally the static electric field distribution is taken into account to optimize the geometry of the cell, but the situation becomes more complicated when the effects are involved of the intense electron beam passing through the cell.

1.1 Effects resulting from the intense electron beam

The existence of intense electron beam brings about the following effects.

Firstly, a large number of the charged particles behave like an electrode, which can change the static E-field distribution and increase the peak field value inside the accelerating gap. Our simulation shows that the change is almost proportional to the intensity of the electron beam. But in fact the above field increase will be counteracted due to beam loading[2].

Secondly, in a normal case there is nearly 10% of the electron beam losing in the beam line transportation[3]. These stray electrons will bombard the accelerating electrodes and generate the secondary electron emissions. However according to the data from Ref. [4], the secondary electron emissions will decay rapidly, since the energy of the stray electrons, normally higher than 1 MeV, corresponds to a multiplication factor smaller than 1. Therefore the impact of the secondary electrons can be neglected in the breakdown modeling.

Furthermore, a kA level intense electron beam will excite a strong wake field when passing through the accelerating gaps. The wake field will not only deflect the electron beam and lead to the beam breakup instability, but also modulate the accelerating field distribution and enhance the risk of high voltage breakdown. In this paper, we will focus on the studies of the wake field and its influence in the accelerating gap.

1.2 The Dragon-I accelerator

The Dragon-I accelerator will be taken as an example to demonstrate the influence of the electron beam in the following sections.

The Dragon-I accelerator is a 20 MeV, 2.5 kA, 90 ns (FWHM) linear induction accelerator operat-

Received 18 December 2007
* Supported by Special National Foundation of China
1) E-mail: zhangkz@caep.ac.cn

ing in a single pulse mode. Its main accelerating section consists of 72 induction cells, and each cell can provide a high voltage pulse of 250 kV, 120 ns (FWHM). A cutaway view of the induction cell is shown in Fig. 1. The electron beam will be accelerated while passing through the bore of the cell, and focused by the solenoid at the same time. The narrow, curved accelerating gap, together with the ferrite materials can damp the transverse wake field effectively.

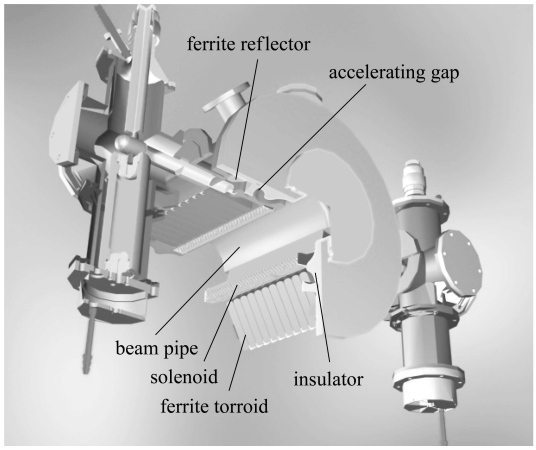

Fig. 1. Cutaway view of the induction cell of Dragon-I accelerator.

2 Fundamental theory

2.1 Wake field expression

The fundamental mode of the wake field, TM_{1n0} mode, is the main concern in an induction accelerator because it has an axial electric field component between the accelerating gap electrodes, and its magnitude increases exponentially in the process of the resonant interaction with electron beam.

The corkscrew[5] is under the control for accelerators like Dragon-I, so there exists nearly no phase difference between the preceding particles which excite the wake field and the tail particles. In this case the motion of the tail particles is disturbed not by the radial magnetic wake field component, B_r, but by the azimuthal field component, B_θ , near the accelerator axis which can be written in the form of the wake function $W_\perp$[6],

$$B_\theta(t)=\frac{1}{cg}\int_0^t W_\perp(t-t')I(t')r(t')\mathrm{d}t' \ , \qquad (1)$$

where,

$$W_\perp(t)=-\frac{Z_\perp(\omega_0)}{Q}\omega_0^2\mathrm{e}^{-\omega_0 t/2Q}\frac{\sin(\omega' t)}{\omega'} \ . \qquad (2)$$

In the above equations, c is the light velocity, r represents the beam centroid, $I(t)$ is the time dependent beam current, g is the gap width, $Z_\perp(\omega_0)$ is the transverse impedance, Q is the quality factor, ω_0 is the resonant frequency of the induction cell, and $\omega'=\omega_0\sqrt{1-1/(2Q)^2}$. The beam current with a rectangular like pulse shape in one induction linac can be described as,

$$I(t)=I_0[1-\exp(-a_1\cdot t)]\cdot\{1-\exp[a_2\cdot(t-t_{\max})]\}, \ (3)$$

where, I_0 is the beam current magnitude, $t_{\max}$ represents the pulse bottom width, a_1 and a_2 are the parameters relative to the front and fall end of the pulse respectively.

In the induction linac of Dragon-I, a_1=3.5/τ, a_2=4/τ, where τ=25 ns refers to the rise time of the pulse, $t_{\max}\approx$110 ns, and $I_0\approx$2.5 kA.

2.2 The motion equation

A model is established to simulate the interaction between the electron beam and the wake field. In this model the beam pulse is cut into numerous slices, therefore the motion of each slice through each cell can be tracked.

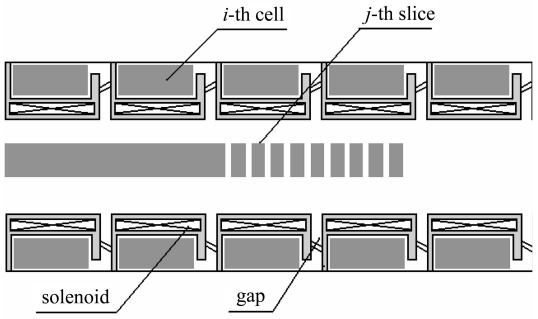

Fig. 2. Schematic of the interaction between electron beam and the cells.

An induction cell can be divided into the drifting section (solenoid) and the accelerating section (gap), as shown in Fig.2. The electron beam will be focused by the solenoid in the drift section. At the exit of the drifting section of the i-th cell, the transverse displacement and transverse momentum of the j-th slices are

$$r_\mathrm{d}(i,j)=r(i-1,j)\cos(k_\beta l)+r'(i-1,j)/k_\beta\sin(k_\beta l), \qquad (4)$$

$$r'_\mathrm{d}(i,j)=-r(i-1,j)k_\beta\sin(k_\beta l)+r'(i-1,j)\cos(k_\beta l), \qquad (5)$$

where $k_\beta=qB/2m_0c\beta\gamma$, β is the relative velocity, γ is the normalized energy, q and m_0 are the charge and mass of an electron respectively. l equals to the cell length approximately since the gap width is too small compared with the length of drifting section. Therefore after the beam crosses the gap, the transverse displacement is negligible, but the transverse

momentum changes result from the kick of the wake field. At the exit of the i-th cell,

$$r(i,j)=r_{\rm d}(i,j)+r_{\rm misalignment}\ , \tag{6}$$

$$r'(i,j)=r'_{\rm d}(i,j)+kick(i,j)+r'_{\rm misalignment}\ . \tag{7}$$

In the above equation the alignment errors of the accelerator are added, and $r_{\rm misalignment}$ and $r'_{\rm misalignment}$ represent the offset and tilt of the cell axis respectively. The *kick* refers to the transverse momentum change,

$$kick(i,j)\ =\ \frac{qg}{m_0\beta\gamma c}B_\theta=\frac{q}{m_0c^2\beta\gamma}\int_0^t W_\perp(t-t')I(t')r'_{\rm d}(t')\mathrm{d}t'\ . \tag{8}$$

In the simulation model the integral is transformed to a sum as

$$kick(i,j)=-\frac{Z_\perp(\omega_0)}{Q}\frac{q\omega_0^2}{m_0c^2\omega'\beta\gamma}\sum_{k=1}^{j}\exp\left((j-k)\frac{\omega_0\Delta t}{2Q}\right)\times\sin(\omega'(j-k)\Delta t)I(k)r'_{\rm d}(i,k)\Delta t\ . \tag{9}$$

Equations from (6,7) to (9) are incorporated into a transmission matrix of the i-th cell, and the electron beam motion is characterized by the multiplication of the matrixes of all the 72 cells. On the other hand the wake field in each cell will be accumulated with more and more electrons crossing the gap.

In the simulation the energy gain $\Delta\gamma$ of electrons passing through each gap is taken into account as well, and at the exit of i-th cell,

$$\gamma(i)=\gamma(i-1)+\Delta\gamma\cdots. \tag{10}$$

2.3 Operating condition and simulation result

The operating condition of Dragon-I accelerator is shown in Table 1 and Table 2. Only the $\rm TM_{130}$ mode is taken into account since it is most dangerous[7].

Table 1. Properties of the Dragon-I accelerator.

symbol	value	unit	comment
n	72		number of the cells
l	0.533	meter	length of a cell. An inter cell is divided into 4 sections, and every section is taken as part of a drift section
ω_0	750	MHz	resonant frequency ($\rm TM_{130}$)
$Z_\perp$	745	Ω/m	transverse impedance($\rm TM_{130}$)
Q	31		quality factor ($\rm TM_{130}$)
$m_0c^2\Delta\gamma$	230	keV	energy gain per gap, in consideration of beam loading
B_0	0.048	T	initial transportation magnetic field, and the field evolves as $B=B_0(\gamma/\gamma_0)^{1/2}$

Table 2. Beam parameters of the Dragon-I accelerator.

symbol	value	unit	comment
$(\gamma_0-1)m_0c^2$	3.5	MeV	the injected beam energy
r_0	1	mm	initial transverse displacement of the beam centroid
r'_0	0.01	rad	initial transverse momentum of the beam

The motion of electron beam and the induced wake field are simulated at the operating condition of the Dragon-I accelerator with $r_{\rm misalignment}$ <0.2 mm and $r'_{\rm misalignment}$ <1 mrad. A three dimensional distribution of the calculated magnetic wake field of $\rm TM_{130}$ mode is shown in Fig. 3, and its maximum is about 0.005 T.

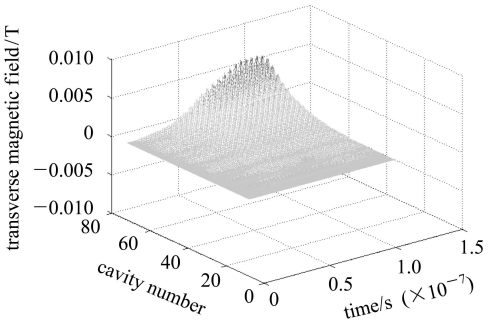

Fig. 3. Distribution of magnetic wake field at the operating condition of Dragon-I.

2.4 The axial electric wake field

The axial electric field component of $\rm TM_{1n0}$ mode near the axis can not be derived in the same way as the transverse magnetic field component, and it tends to be deduced from the magnetic field already known, since the electric field is zero at the axis, but the magnetic field reaches its maximum.

The induction cell can be taken as a pill-box, and the field components expression of $\rm TM_{1n0}$ mode in such a cylinder[8] characterizes the relation between the electric field and magnetic field,

$$B_\theta=D\frac{\omega_0}{c^2}J'_1\left(\frac{u_{1n}}{a}r\right)\cos\theta\sin(\omega_0t+\phi), \tag{11}$$

$$E_z=D\frac{u_{1n}}{a}J_1\left(\frac{u_{1n}}{a}r\right)\cos\theta\cos(\omega_0t+\phi), \tag{12}$$

where D is the constant, u_{1n} is the n-th root of the first order Bessel function, a is the effective radius of the cylinder, and a=0.65 m for the induction cell of Dragon-I.

Taking the maximum magnetic field of 0.005 T into Eqs. (11,12), the distribution of the axial electric field and transverse magnetic field along the radius inside the gap can be drawn, as shown in Fig. 4. The maximum electric field is about 17 kV/cm, and located at r=12 cm, around one of the peak points of the static electric field, and the corresponding peak field strength is 207 kV/cm.

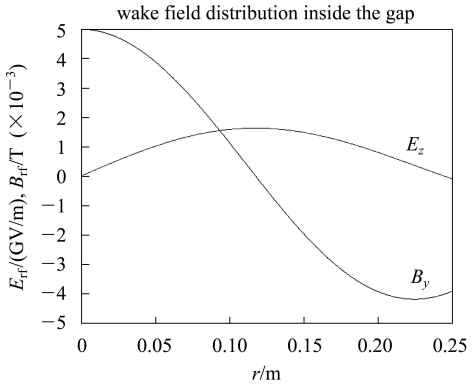

Fig. 4. The field distribution of TM_{130} mode inside the induction accelerating gap.

3 Influence on the high voltage property

The breakdown phenomena can be divided into two stages, the field emission, and the particles motion in succession[9].

In the first stage, the electron emission density is given by Fowler-Nordheim (F-N) formula[10], but there exists a little difference for static (DC) fields and wake (RF) fields. The dependences of emission current on the electric fields are shown in Fig. 5, where the field enhancement factor β=70.

At the same field strength, the RF emission is much lower than DC emission. On the other hand, since the emission density increases exponentially with the electric field, if the DC field (e.g. 207 kV/cm) is strengthened by the RF field (e.g. 17 kV/cm), the incremental emission density becomes noticeable, which is more than 10 times the DC emission.

In the second phase, the electrons will be accelerated by the static field, but modulated by the wake field at the same time. The accelerating field will be reinforced or weakened by the wake field at different initial phases, which results in the variation of the transit time. Meanwhile the transverse motion direction changes periodically as the initial phase changes from 0° to 360°.

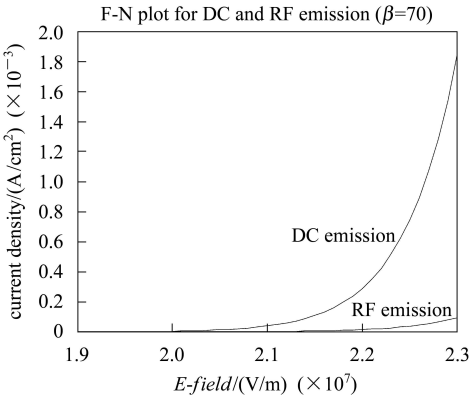

Fig. 5. F-N plot for DC and RF emission (β=70).

Further investigation shows in the vicinity of the operating condition, the electric wake field brings forth no remarkable influences on the motion of electrons since the wake field is too lower than the accelerating field.

4 Conclusion

Considerable axial electric wake field will be excited inside the induction accelerating cell, for example, 17 kV/cm at the operating condition of Dragon-I. Since the high voltage property will be influenced by this wake field more or less, its effect should be taken into account before the operating accelerating voltage is fixed.

References

1 WANG Hua-Cen, ZHANG Kai-Zhi, WEN Long et al. Proceedings of the 1999 Particle Accelerator Conference. New York, 1999. 3263—3265
2 Ong M M. Proceedings of International Pulsed Power Conference. Monterey, 2005. 112—115
3 DING Bo-Nan et al. HEP & NP, 2005, **29**(6): 604 (in Chinese)
4 Robert J B, Edl S. High Power Microwave Sources and Technologies. Wiley-IEEE Press, 2001
5 CHEN Y J. Nucl. Instrum. Methods in Physics Research A, 1990, **292**: 455—464
6 ZHANG Kai-Zhi. Research on Beam Breakup Instability of Linear Induction Accelerator. Beijing, 2000 (in Chinese)
7 ZHANG Kai-Zhi, WANG Hua-Cen, ZHANG Wen-Wei et al. Proceedings of 13th International Conference on High-Power Particle Beams (BEAMS 2000). Nagaoka, Japan, 2000, 548—551
8 SHEN Zhi-Yuan. Microwave Technology. National Defense Engineering Press, 1980 (in Chinese)
9 Wilson P B. Proceedings of XXth International Linac Conference. Monterey, California, 2000. 618—620
10 Loew G A, WANG J W. RF Breakdown Studies in Room Temperature Electron Linac Structures, SLAC-PUB-4647. 1988